ingegneria sismica
International Journal of Earthquake Engineering
Anno XLIII - Num. 1 - 2026

Multi-objective optimization of energy management strategies for hybrid vehicles

Quan Huang[1,*]

[1] School of Intelligent Manufacturing Engineering, Guangxi Electrical Polytechnic Institute, Nanning, Guangxi, 530299, China

SUMMARY: *The technology of energy management strategy plays an important role in the field of hybrid cars. This paper mainly studies the issue of energy management strategy, which aims at building up a hybrid vehicle simulation model involving vehicle longitudinal dynamics, engine, generator, drive motor, and power battery of parallel hybrid vehicles. On the basis of the simulation model, the basic energy circulation ways are studied, and according to which the optimization objective function is formulated and the initial equivalent factor is taken as the design variable to be optimized. Furthermore, through optimizing the initial equivalent factor calculating coefficient, engine starting torque and transmission main reduction ratio, under the condition that the SOC of power battery is restricted to [-3%,3%], the hybrid vehicle multi-objective optimization model on energy management strategy is built by means of the multi-objective particle swarm optimization algorithm. In simulations, an engine torque fluctuation constraint model is also added, which can turn the engine power fluctuation into equivalent fuel consumption to achieve the purpose of further enhancing the vehicle performance under the energy management strategy. According to the hybrid vehicle energy management strategy multi-objective optimization model proposed in this paper, the optimal solution set of energy management strategy is gained. Not only can it effectively improve engine working efficiency, keeping the efficiency of engine within the range of 0.20-0.35, but also can reach 9.82% improvement of the whole vehicle fuel economy on average.*

KEYWORDS: *Energy management strategy; Multi-objective optimization model; Multi-objective particle swarm optimization; Engine torque fluctuation; Hybrid electric vehicle*

1 Introduction

As fossil fuels become increasingly scarce and the pressure from the environment intensifies, many countries in the world are implementing tougher standards on the emissions of passenger cars beyond their current policies [1, 2]. The requirements placed on the automotive industry in terms of energy consumption and emission levels are becoming increasingly stringent in the international context. While China's New Energy Vehicle Industry Development Plan (2021-2035) serves to expand the framework of its previous Energy-Saving and New Energy Vehicle Industry Development Plan (2012-2020), it is also the strategy map to guide its future development of new energy vehicles. In the United States, the Environmental Protection Agency has issued regulations mandating the emissions of

*HUANGQUAN2026@163.com
https://doi.org/10.65102/is2026406
Published: 30 April, 2026

light-duty trucks be reduced from 10 mg/m³ in 2017 to 3 mg/m³ by 2021 [3, 4]. For China, the regulation called “Emission Limits and Measurement Methods for Pollutants from Light-Duty Vehicles (China Stage VI)” reduces particulate matter emissions by 67%, while for the first time introducing particulate number limits, thus setting new requirements for controlling emissions of light-duty vehicles with gasoline engines [5-7]. Moreover, some countries around the world are considering banning the sale of traditional fuel-powered vehicles [8, 9]. Under such circumstances, the passenger cars powered only by internal combustion engines will not be able to satisfy the needs of the automobile market in the future. HEV, fuel cell, and purely electric cars can be considered alternative choices to traditional passenger cars [10-13].

Nonetheless, there are quite some difficulties facing FCVs mainly because of the extremely harsh conditions of operations in the membrane electrode assemblies (MEA) of the vehicle. The need for proper water management and thermal management has been identified while significant temperature gradients at various points within the MEA affect the service life. Another major issue associated with the development of fuel cell vehicles is related to the hydrogen storage on board and the hydrogen fueling infrastructures [14-17]. In addition, the development and utilization of electric cars are hindered by several issues including; low energy density of onboard batteries which are not easy to increase in the short run, short life service, short driving range after charging, high cost of purchase and costly maintenance [18-20]. The HEV technology combines the following main benefits of energy efficiency, environmental protection, longer mileage range and power performance. It utilizes two or more sources of power, with the battery pack or super capacitor electric motor taking the place of the engine under situations when the engine operates inefficiently. It, therefore, ensures that there is energy conservation and low emissions. As a result, hybrid electric vehicles have become very popular [21-24]. Nonetheless, the dual usage of an engine together with an electric drive leads to a relatively complicated structure and requires advanced control technology [25, 26]. Energy Management System (EMS) constitutes the core element of the control of new energy vehicles. Strategy for EMS is among the crucial research areas of HEVs since it makes sure that motor controls the operating point of the engine thus keeping the engine running at high-efficiency zones, hence saving fuel [27, 28].

HEVs have an engine and energy storage unit as dual sources of energy. When the vehicle is in use, the energy requirement should be divided between these two sources, and how this division should be done becomes the key issue in the development of EMS. Reference [29] uses the K-means algorithm for developing a rule-based multi-objective optimization EMS, which not only reduces the use of hydrogen but also increases the life of the fuel cell. Its real-world results deserve consideration. [30] has used the particle swarm optimization-based multi-objective EMS for the power-split HEV. The above is mainly achieved through optimizing certain important ECMS parameters and incorporating penalty function to realize the balance of the current state of charge. Consequently, the reduction in the fuel consumption of the vehicle is within the range of 7.7% to 9.8%. Considering that there exist trade-offs between energy consumption, environmental impact and battery lifetime in HEVs, Reference [31] seeks to balance the three factors. In this case, reference uses multi-objective particle swarm optimization algorithm and dynamic programming algorithm to design hybrid point-line energy management system that improves energy consumption, emission reductions and increases battery life. The use of genetic algorithm by reference [32] to compute battery charging/discharging criteria under three states, which include minimum hydrogen consumption rate, battery charge retention rate and fuel cell efficiency depending on different road driving situations, leads to rule-based real-time energy management system design.

Reference [33] designs two parallel HEV-EMSs using multi-objective genetic algorithm in order to improve the fuel economy, electrical system efficiency, battery performance and increase its life. Compared to traditional rule-based methods of EMS, the designed strategy improved significantly the battery performance and resulted in reduced fuel consumption. Reference [34] proposes an efficient multi-objective global optimization algorithm for series-parallel plug-in HEV-EMS by integrating ladaw pseudo-spectrum connection method and non-dominated sorting genetic algorithm for optimizing energy savings and battery lifetime in suburban driving environments. There have been reported energy saving percentage rates ranging between 26.74% to 53.87%.

Optimized point line methodology, which includes rule based and multi-objective optimization approaches, is proposed in Ref. [35] to develop a multi-objective adaptive EMS for HEVs. In doing so, operating costs and fuel cell lifetime depreciation are both decreased by 35.3% and 42.15%, respectively, and at the same time, battery operational efficiency is improved. Ref. [36] proposed an EMS for power split HEV by incorporating multi-objective optimization approach with explainable artificial intelligence (dual layer random forest EMS). The EMS takes into account power consumption, fuel consumption, battery depreciation, and engine start-stop counts. Thus, a significant decrease is achieved in all of the latter indicators. Ref. [37] describes a multi-objective optimized EMS for HEVs with hybrid energy storage systems, focusing on balancing the relationship between fuel efficiency and battery life when accelerating and braking. As a result, fuel consumption decreases by 18.9%. Ref. [38] presents a real-time multi-objective EMS for HEVs using the battery lifespan as a guiding principle. Fuel efficiency, electrical energy consumption, and battery depreciation are among the optimization objectives. In addition to cutting down the total cost of operations by 6.15%, the design of the model using short-term speed prediction models and MPC reference trajectory planning was able to attain 98.17% dynamic planning efficiency. According to [39], an EMS for HEVs using MPC that is both health-aware and multi-objective optimized is presented, aiming at extending the lifespan of the batteries. The proposed scheme is able to reduce economic costs by up to 50% at certain speeds and cut down energy consumption levels. In [40], Pontryagin's minimization principle, dynamic programming, and Gaussian process regression model are used to design a hybrid integer nonlinear MPC-based EMS. Hybrid MPC (model predictive control) is one of the strategies presented in Reference [41] to optimize HEV energy management in terms of rule-based control and ECMS. The strategy allows for the real-time execution while lowering the amount of fuel consumption and enhancing the quality of pollutant emissions. It outperforms ECMS due to its flexibility and efficiency.

Reference [42] presents EMS strategies based on reinforcement learning (RL) methods, including Q-learning, Deep Q-Network (DQN), and Deep Deterministic Policy Gradient (DDPG). Such methods pay attention to the issues of fuel economy and fuel cell endurance; hence, the use of RL could be promising due to the continuous development of the technology. Reference [43] proposes EMS based on Q-learning technique for HEV buses; this strategy successfully solves issues of fuel economy, state-of-charge maintenance, power fluctuation of the fuel cell system, and fuel cell lifetime. Reference [44] uses Deep Q-learning method combined with strongly convex objective function optimization and provides a new EMS for range-extended HEV cars. It uses predictions about driving cycle and driving conditions in the process of neural network-based predictive control to provide a solution for the improvement of adaptability under the changes of the environment, which leads to 30% better adaptability and 18% decrease in fuel consumption. In Reference [45], authors suggest an adaptive optimization of the ECMS strategy, which helps to improve energy management in case of PHEV cars; their approach is mainly based on dual DQN and driving cycle data.

Reference [46] presents an EMS for HEV, which is based on DQN and competitive DQN; they help to increase fuel economy by 94.28% and 95.7%, respectively. Test results were conducted based on Chinese truck driving conditions. Reference [47] introduces a self-optimizing power matching EMS for HEVs considering the aspects of energy efficiency and battery aging by applying DDPG. Paper [48] discusses plug-in HEVs by developing an EMS based on DDPG for the electric drive system, taking into account the thermal behavior of the electric drive system. Through the developed EMS, the battery and motor temperatures are regulated, the energy management is optimized, HEV operation stability is ensured, and a decrease in fuel consumption of 8.46% is achieved. Paper [49] develops a multi-objective optimization of HEV-EMS with the help of a multi-agent reinforcement learning model. Within such a framework, where the engine and battery serve as two cooperating agents, optimal allocation of powers and controls are reached, leading to a decrease in fuel consumption of 17.66%.

The research starts with modeling of the key system structure of parallel hybrid vehicles and then analyzes the four energy flow modes that exist in parallel hybrid vehicles. Then, an objective function for the energy management strategy is established and multi-objective optimization of multiple decision variables is performed while setting relevant constraints so that a multi-objective optimization model for energy management strategy of hybrid vehicles can be designed. Multi-objective particle swarm optimization algorithm is used as the optimization solution method, which is described step-by-step to implement the multi-objective optimization for energy management strategy of parallel hybrid vehicles. Finally, performance of the hybrid vehicle will be examined in terms of power and economic aspects, and frequency of engine torque fluctuations will be optimized so as to minimize torque fluctuation. Simulation experiments will be carried out to confirm the effectiveness of the developed multi-objective optimization model for improving energy management strategy of parallel hybrid vehicles.

2 Modeling of Parallel Hybrid Vehicles

In this section, the modeling of the car model for a PHEV is proposed. The structure of this type of car mainly includes an engine, generator, front drive motor, rear drive motor, and power battery. Considering the emphasis of this research on the economical aspects of PHEVs, the power supply for the front and rear drive motors will be allocated equally.

2.1 Vehicle Longitudinal Dynamics Model

The balance relationship between the vehicle's driving force and various resistive forces during operation must satisfy the equilibrium condition shown in Equation (1).

$$F_d = F_f + F_w + F_i + F_a \tag{1}$$

In the equation, F_d represents the vehicle driving force; F_f represents rolling resistance; F_w represents air resistance; F_i represents gradient resistance; F_a represents acceleration resistance. Expanding the resistances in Equation (1) yields Equation (2):

$$F_d = mgf\cos\theta + 0.5\rho A C_d v^2 + mg\sin\theta + \delta m\frac{dv}{dt} \tag{2}$$

In the equation, m represents the vehicle mass; g denotes gravitational acceleration; f is the rolling resistance coefficient; θ indicates the road gradient; ρ signifies air density; A denotes the frontal area; C_d represents the drag coefficient; v indicates vehicle speed; and δ denotes the vehicle's rotational mass coefficient.

2.2 Engine Model

The information regarding the engine used in this paper comes from engine bench test results. Once an input consisting of the engine's rotation speed and torque is sent to the engine model, the model searches the engine fuel consumption map to find out the related fuel consumption, as illustrated in Equation (3):

$$m_{fuel} = f\left(T_{eng}, \omega_{eng}\right) \tag{3}$$

In the equation, m_{fuel} represents the engine fuel consumption value; T_{eng} denotes the engine torque; ω_{eng} indicates the engine rotational speed.

2.3 Generator Model

Because the method introduced in this paper mainly focuses on the consumption behavior of the vehicle, the model of the generator is assumed to be in its steady-state operation. This means that the thermal and electrical effects of the motor are not considered and that the generator is assumed to be able to react quickly to the command for torque generation. The power produced by the generator can be written in Equation (4):

$$\begin{cases} P_{gen} = T_{gen}\omega_{gen} / \eta_{gen} \\ \eta_{gen} = f\left(T_{gen}, \omega_{gen}\right) \end{cases} \tag{4}$$

In the equation, P_{gen} represents generator power; T_{gen} represents generator torque; ω_{gen} represents generator rotational speed; η_{gen} represents generator efficiency.

2.4 Drive Motor Model

The drive motor model, similar to the generator model, has also been appropriately simplified. The power calculations for the front and rear drive motors are shown in Equation (5):

$$\begin{cases} P_m = \begin{cases} T_m\omega_m / \eta_m, T_m\omega_m > 0 \\ T_m\omega_m\eta_m, T_m\omega_m < 0 \end{cases} \\ \eta_m = f\left(T_m, \omega_m\right) \end{cases} \tag{5}$$

In the equation, P_m represents the drive motor power; T_m denotes the drive motor torque; ω_m indicates the drive motor rotational speed; and η_m signifies the drive motor efficiency.

2.5 Power Battery Model

Power batteries are an important component in the powertrain structure. In this study, a power

battery comprises 100 cells that are joined in parallel connection. Power battery modeling is done through the R-int model, which considers the battery as a source of voltage that is connected to a resistor in parallel. Open circuit characteristics of the cell voltage and its resistance are shown in Figure 1 below.

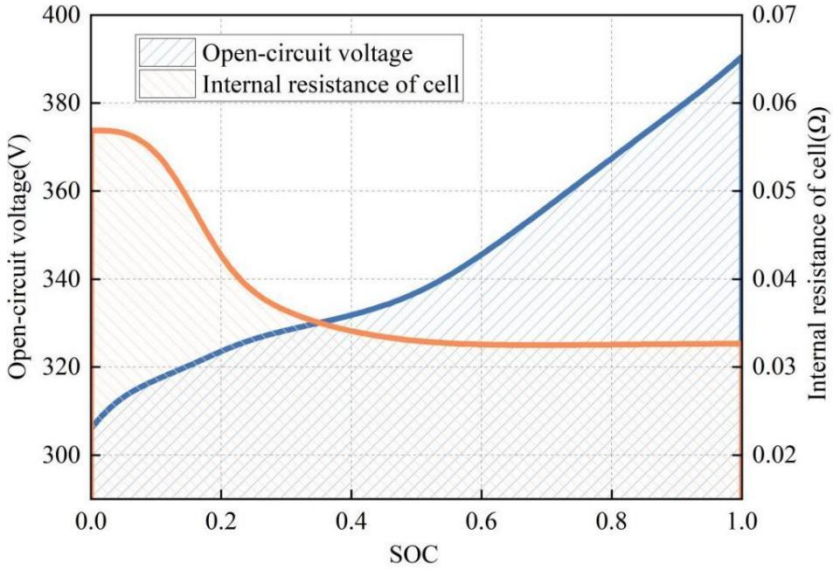

Figure 1: Characteristics of Battery OCV and Resistance

The mathematical expression for determining the State of Charge of a battery based on the existing method of integrating current will be as expressed in Equation (6):

$$SOC(t) = SOC_i - \frac{1}{Q_{bat}} \int_0^t I_b(t) dt \tag{6}$$

In the equation, SOC_i represents the initial battery SOC state; Q_{bat} denotes the battery capacity; $I_b(t)$ indicates the battery output current. The calculation of $I_b(t)$ is given by Equation (7):

$$I_b(t) = \frac{U_{oc}(t) - \sqrt{U_{oc}^2(t) - 4R_{\text{int}}(t)P_{bat}(t)}}{2R_{\text{int}}(t)} \tag{7}$$

From the above equations, $U_{oc}(t)$ denotes battery OCV; $R_{\text{int}}(t)$ denotes battery internal resistance while $P_{bat}(t)$ stands for battery output power. This paper utilizes a semi-empirical approach to build battery life cycle model expressed in Equation (8). The factors considered include charge/discharge rate, temperature, and State of Charge.

$$\begin{cases} Q_{loss} = B\exp\left(\dfrac{-E_{act} + \xi I_c}{R\left(T_{bat} + 273.15\right)}\right) A_h = \\ B = \alpha SOC + \beta \\ I_c = \dfrac{|I_b|}{Q_{bat}} \end{cases} \tag{8}$$

In the equation, Q_{loss} represents the percentage of battery capacity loss; B denotes the pre-exponential factor; E_{ad} is the activation energy; ξ is the correction factor; I_c indicates the battery charge/discharge rate; R is the molar gas constant; T_{bat} is the battery temperature; A_h is the cumulative charge throughput; z is the power exponent factor; α and β are constant terms.

End of life (EOL) of batteries refers to when there is a loss of capacity by 20 percent. Rated life of the battery refers to the battery capacity throughput at its EOL and is based on equation (8), giving us equation (9):

$$\Gamma = \left[\frac{20}{B \exp\left(\frac{-E_{act} + \xi I_{c,nom}}{R\left(T_{bat} + 273.15\right)} \right)} \right]^{\frac{1}{z}} \tag{9}$$

In the equation, $I_{c,nom}$ represents the battery charge/discharge rate under rated conditions. Relative to the battery's rated operating conditions, the influence factor $\sigma\left(I_c, \theta, SOC\right)$ quantifies the impact of actual operating conditions on battery aging, as expressed in Equation (10):

$$\sigma\left(I_c, \theta, SOC\right) = \frac{\Gamma}{\gamma\left(I_c, \theta, SOC\right)} = \frac{\int_0^{EOL} \left| I_{c,nom}(t) \right| dt}{\int_0^{EOL} \left| I_c(t) \right| dt} \tag{10}$$

In the equation, $\gamma\left(I_c, \theta, SOC\right)$ represents the total charge flowing through the battery at end-of-life under actual operating conditions. Within the EMS, battery aging costs are expressed in terms of effective capacity as shown in Equation (11):

$$A_{eff}(t) = \int_0^t \sigma\left(I_c, \theta, SOC\right) \left| I_b(t) \right| dt \tag{11}$$

In the equation, $A_{eff}(t)$ represents the effective charge flowing through the battery. When $A_{eff} = \Gamma$, the battery is considered to have reached end-of-life. Therefore, battery aging can be mitigated by reducing the effective charge.

3 Multi-Objective Optimization Energy Management Strategy

3.1 Modes of Operation of Parallel Hybrid System

The type of hybrid system being discussed here is a parallel hybrid system, which is described in the figure 2 below.

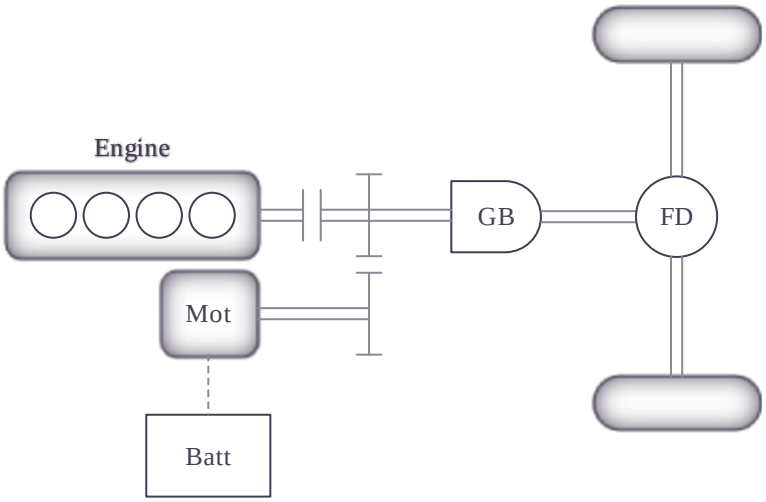

Figure 2: Parallel hybrid configuration P2

There are four energy flow modes in total:

(1) Motor-only drive mode.

This type of system is appropriate for the operations of vehicles at start-up or under low load conditions. This is because, in such cases, the power battery provides the energy and supplies electricity to the motor. Power and torque are then transmitted by the motor to the transmission via the output shaft of the transmission.

(2) Engine-only drive mode.

This drive mode is mainly utilized during the medium to high load periods after starting the vehicle. At this point, the vehicle requires a higher amount of torque, which means that the engine will be operating near its optimum operational range. Driving the engine at its optimum range helps minimize the amount of fuel consumed and emissions from the vehicle. The engine can be driven depending on the battery's state of charge (SOC) to generate excess energy to increase its power generation by a certain percentage, and the excess energy generated is channeled to the generator to generate electrical energy and charge the battery. In this drive mode, the engine is the main source of power in the hybrid vehicle. Speed and torque generated by the engine are fed into the input of the transmission system through the clutch, and then the speed is lowered while the torque is increased to drive the shaft. During charging, some shaft energy is diverted to drive the generator to generate electrical energy, which is charged into the power battery.

(3) Engine/Motor Combined Drive Mode.

This operation is designed for scenarios involving heavy loading such as uphill drives and transportation of heavy loads. Where the engine alone cannot handle the required driving force, the electric motor is brought in as a secondary source of power. In this case, both the engine and the motor work together to provide the motive power. The power produced by the engine's output shaft is delivered via the clutch and combined with that of the motor's output shaft before being delivered to the transmission mechanism. This mechanism reduces speed and boosts torque to transfer shaft power to the final drive and the wheels. The motor derives its power from the power battery in this operation.

(4) Brake Energy Recovery Mode.

The brake regeneration mode operates when there is a need for deceleration and braking. It starts when the driver presses the pedal down. The control system analyzes the state of charge (SOC) of the power battery, and once the SOC is below the maximum point, the brake regeneration operation can start. The negative torque generated during braking is transmitted through the wheels, main reduction gear, and transmission to the motor. The motor is forced

to rotate, cutting through magnetic field lines to generate electricity that charges the power battery. When the driver presses the brake pedal, if the required braking force exceeds the force needed to drive the motor for power generation, the mechanical braking system engages. Excess braking force is dissipated as thermal energy through the brake calipers.

3.2 Development of Multi-Objective Optimization Models

3.2.1 Optimization Objective Function

These are the steps of the optimization process used in this research:

(1) Optimize the objective function by establishing an objective function with fuel consumption and emissions as dependent variables.

(2) Decision variables: In the established hybrid system, initial equivalent factor s_0, equivalent factor calculation coefficients c_1, c_2, engine starting torque T_{strat}, and main reduction ratio i of the drive shaft are selected as decision variables.

(3) Constraints: In its most usual form of transportation, vehicles need to have the capacity to adjust themselves according to changing terrain, hence making power constraints essential to the system. These would include acceleration from 0 to 100 km/h, acceleration from 40 to 100 km/h, and satisfactory hill-climbing capacity. Another important constraint is the state of charge of the battery which forms part of the vehicle itself. It should be noted that HEVs do not require electrical inputs from any outside source as plug-in HEVs do. Hence, the state of charge of the battery at the end of a typical driving cycle should be constant to its initial value or vary very little.

Based on the above steps, the optimization objective function is first established as shown in Equation (12):

$$\min[f(fuel); f(CO); f(HC); f(NOx)] \tag{12}$$

Among these, $f(fuel)$ represents the fuel consumption of the engine during one cycle, measured in milligrams; $f(CO)$, $f(HC)$, $f(NOX)$ denote the cumulative CO, HC, and NOx emissions during one cycle, respectively, measured in milligrams.

3.2.2 Optimization of Decision Variables

Hybrid systems are strongly coupled nonlinear systems where the value of an optimization objective function is often influenced by multiple decision variables. Optimizing all decision variables sequentially during system optimization would result in an enormous computational burden, making it impractical. Therefore, for certain decision variables with minimal impact on the optimization objective function, this paper excludes them from consideration. Only those decision variables exerting significant influence on the optimization function are selected for optimization as follows:

(1) Initial equivalent factor s_0.

To enhance the ECMS strategy's adaptation to the WLTC cycle and differentiate it from rule-based energy management strategies in terms of fuel consumption and pollutant emission control, the equivalent factor s within the ECMS strategy is first selected as one of the design variables for multi-objective optimization. Within the ECMS strategy, the equivalent factor represents the cost coefficient converting electricity consumption into fuel consumption. As the equivalent factor increases, the fuel consumption equivalent to a given amount of electricity consumed also increases. This indicates insufficient power, prompting the control strategy to prioritize charging the traction battery. In the ECMS strategy developed herein, the

equivalent factor adapts dynamically based on operating conditions. While its value fluctuates throughout the test cycle, the initial equivalent factor requires manual specification, significantly influencing the strategy's initial control phase. Therefore, the initial equivalent factor s_0 is designated as a design variable.

(2) Calculation coefficients c_1, c_2 for the equivalent factor.

Within the ECMS strategy, the equivalent factor calculation is influenced by formula (13):

$$s(t) = s_0 - c_1 \cdot \left(SOC(t) - SOC_{ref} \right) - c_2 \cdot \int_0^t \left(SOC(t) - SOC_{ref} \right) \cdot dt \tag{13}$$

Here, s_0 denotes the initial value of the equivalent factor s at the start of the cycle; $SOC(t)$ represents the current SOC value of the power battery; SOC_{ref} denotes the target value for the terminal SOC of the power battery. Since the hybrid system studied in this paper is a non-plug-in hybrid system, all electrical energy for the power battery originates from the engine's combustion of gasoline. To ensure the power battery maintains sufficient charge to sustain vehicle operation under any conditions, the target is for the power battery's SOC value to remain near its initial value at the end of each driving cycle. Here, SOC_{ref} denotes the target SOC value for the terminal power battery, typically set within -10% of the initial value; The coefficient c_I corrects the current equivalent factor $s(t)$ based on the difference between the current power battery SOC and the terminal target power battery SOC; The coefficient c_2 corrects the current equivalent factor $s(t)$ by integrating the difference between the current SOC of the power battery and the target SOC of the power battery.

(3) Engine starting torque T_{strat}.

The ECMS strategy incorporates a torque limit to prevent frequent engine starts. Such a value will be used for the design of the conditions for the engine start, and the correct design is of great importance for ECMS. In case of setting the limit at a too low level, the engine will start too often and the vehicle may work in modes with low speed and load; it will be harmful to its fuel consumption and pollutant emissions. In case of a very high limit value, the load factor of the motor will increase and cause the extra discharge of the power battery. Hence, the reasonable design of the starting torque of the engine is necessary.

(4) Main Reduction Ratio i of the Drive Shaft.

When it comes to the dual-shaft parallel hybrid system, it is obvious that the speeds of the engine and motor depend on the speed of the wheels, i.e., the vehicle speed. It is important to state that the main reduction ratio greatly affects the engine's operational range of speed. The optimal choice of the main reduction ratio will allow using the engine in its most efficient zone, and hence save fuel and reduce emission.

3.2.3 Formulation of Constraints

The SOC of the power battery is frequently taken as an assessment criterion in the control strategy of non-plug-in hybrid systems. The control strategy typically strives to keep the maximum value of the SOC variation below 3%, while the SOC at the conclusion of a driving cycle should lie within ±3% of its starting point value. Therefore, the power battery SOC becomes a restriction in this optimization procedure. Within the context of the model employed in this study, the SOC value of the power battery is initially fixed at 80%. The SOC restriction can then be defined using Equation (14):

$$-3\% < \Delta \mathrm{SOC} < 3\% \tag{14}$$

3.3 Optimizing Algorithm Workflow

Multi-objective particle swarm optimization represents a method that extends particle swarm optimization into the field of multi-objective issues. As a result of the many similarities between particle swarm optimization and evolutionary algorithms, such as collaborative searching and communication of information throughout the search procedure, the two strategies have a significant number of similarities in their general problem-solving methods. However, differences exist: multiple optimal positions may coexist within the population, and multiple particles may achieve their own optimal positions during iterations. Consequently, selecting between G_{Best} and P_{Best} requires specific strategies. More importantly, MOPSO maintains external archives for both G_{Best} and P_{Best}, a feature absent in multi-objective evolutionary algorithms. This necessitates MOPSO to consider archive size and diversity when managing these external archives. Additionally, due to the introduction of the external archive concept, the velocity and position update formulas in MOPSO differ slightly from those in PSO, as shown in Equations (15)-(16):

$$VEL[i+1] = W \times VEL[i] + R_1 \times \left(P_{Best}[i] - POP[i]\right) + R_2 \times (REP[h] - POP[i]) \tag{15}$$

$$POP[i+1] = POP[i] + VEL[i] \tag{16}$$

In the formula, REP denotes the external archive set composed of non-dominated solutions. Particles are selected from REP to form G_{Best}. The following outlines the basic execution process of Pareto-based MOPSO:

(1) Initialize particle velocity $VEL[i]$ and particle position $POP[i]$. Compute the fitness function for each particle and add non-dominated solutions to the external archive REP.

(2) Randomly update the initial G_{Best} and P_{Best} of particles.

(3) Ensure particles move within the search space while adjusting their individual optimal solutions by calculating each particle's fitness function based on its movement trajectory.

(4) Maintain the external REP archive based on the new non-dominated solutions while selecting a new G_{Best} for the population.

(5) Check if the termination condition is met. If not, return to step (3). If met, output the results.

The basic execution flow of Pareto-based MOPSO is illustrated in Figure 3.

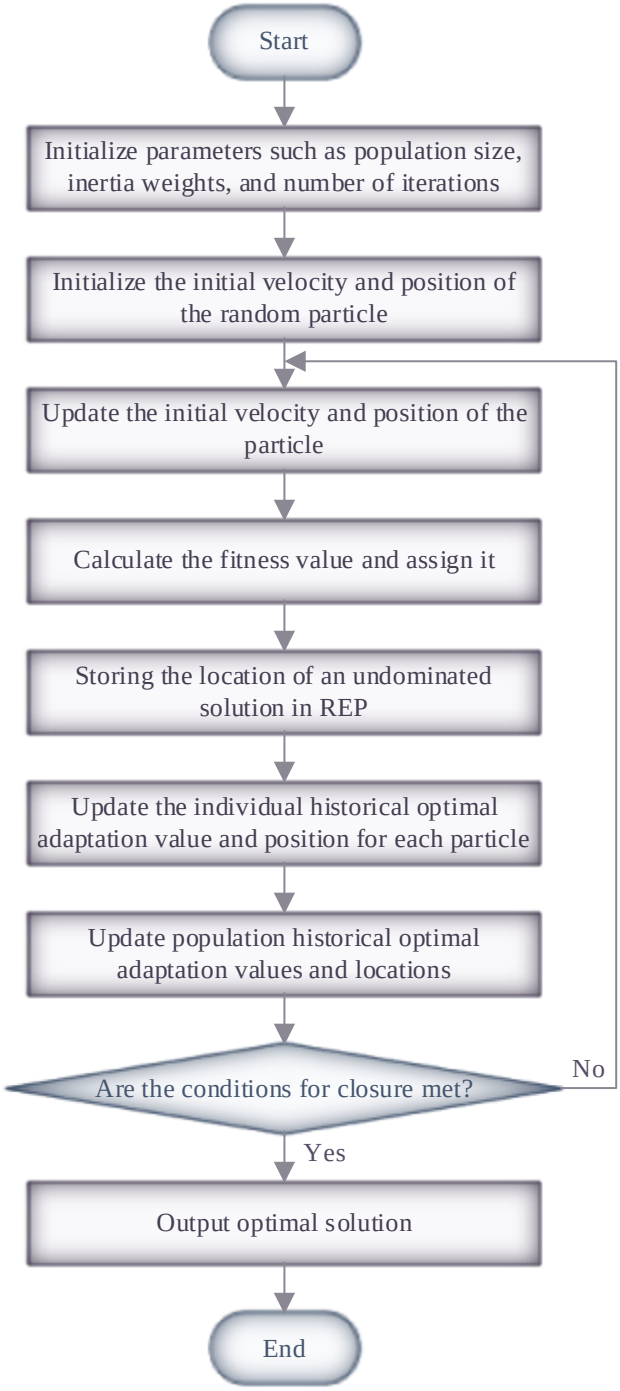

Figure 3: Multi-objective optimisation flowchart

4 Validation of Energy Management Strategies Based on Multi-Objective Optimization Models

The main components of this chapter are: (1) simulation test for the validation of the power performance and fuel consumption of the hybrid vehicle with the use of the proposed energy management method; (2) tests to solve the issue of excessive torque variations due to the

optimized energy management method; and (3) the results and analysis of the multi-objective optimization model.

4.1 Whole Vehicle Performance Validation

4.1.1 Verification of Power Performance

According to the vehicle characteristics and its power performance requirements, the top speed of a parallel hybrid vehicle in a fully loaded mode should be no less than 90 km/h, the max gradeability in fully loaded mode should be no less than 20%, and the acceleration time from 0 to 50 km/h in a fully loaded mode should not exceed 50 seconds. While testing the max acceleration time and speed, the open state of the engine throttle valve is considered equal to 100%. For maximum gradient verification, the operating condition speed is set to 5 km/h, the transmission gear is set to 1st gear, and the gradient is set to 20%. Based on the above performance metrics and simulation validation settings, the vehicle model simulation results are shown in Figure 4: maximum speed and gear performance in (a), gradeability performance in (b), and 0-50 km/h acceleration time with gear performance in (c).

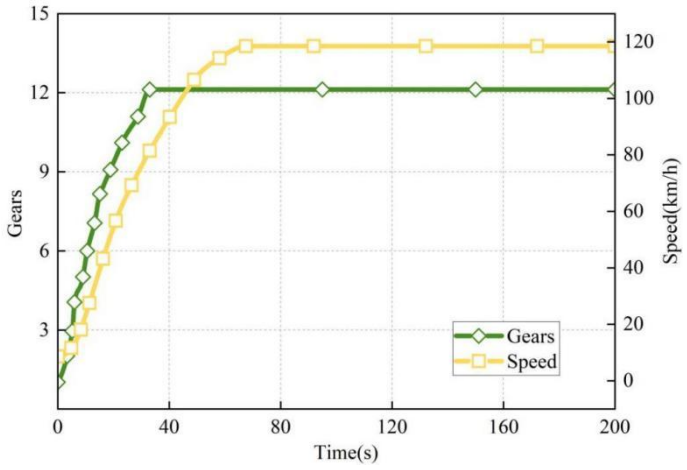

(a) Maximum speed and gear

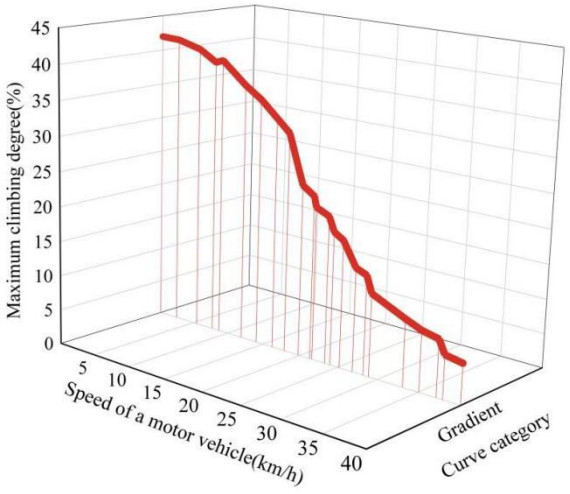

(b) Slope curve

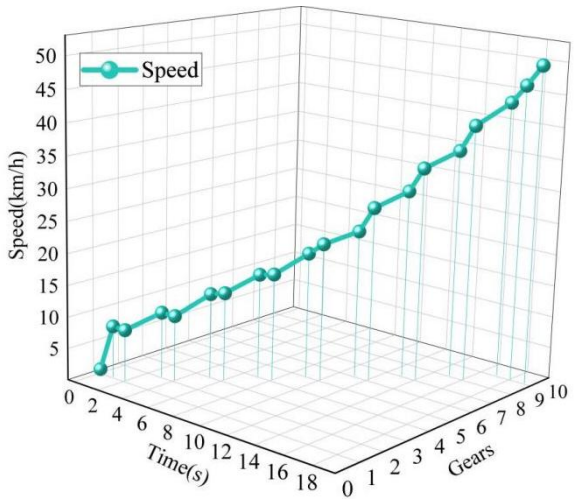

(c) 0-50km/h acceleration time and gear

Figure 4: Power performance Verification Results

From Figures 4(a)-(c), the curve of the maximum speed shows that the hybrid vehicle attains its top speed of 119.37 km/h, thereby achieving the objective of the minimum maximum speed greater than or equal to 90 km/h. From the speed-maximum gradient curve, the maximum gradient attainable from the hybrid train was calculated as 42.73% at a speed of 10 km/h, and it achieves the target of the maximum gradient of 20%. Finally, from the 0-50 km/h acceleration time curve, it can be seen that the acceleration time attained is 19 s, below the target time of 50 s.

4.1.2 Economic Performance Verification

The operating condition selected for the analysis of this paper is the C-WTVC full-load test cycle. The full load operation cycle simulates the complete drive pattern of cars in urban, suburban, and highway drives using the transient speed curve. The operating speed (S1) of the car model designed and the following speed (S2) have been plotted on figure 5. As can be seen from the figure below, the operating speed (S1) is close to 100% overlap with the following speed (S2).

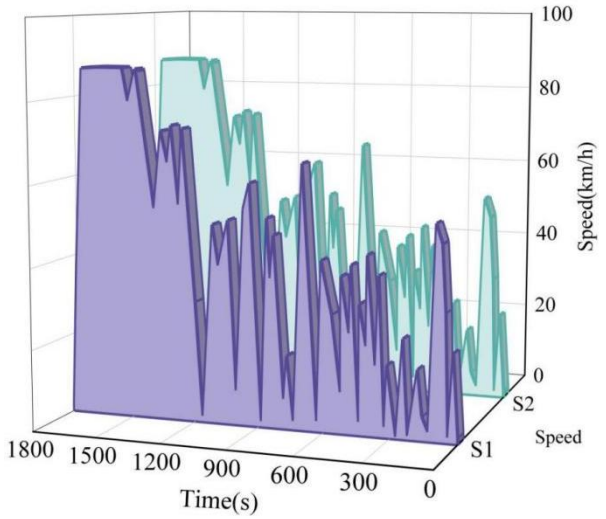

Figure 5: Variation of operational speed with following vehicle speed

Meanwhile, the economic performance of the hybrid railcar adopting the energy management strategy from the multi-objective optimization model in this paper is simultaneously tested. The performances of power distribution are presented in Figure 6(a), the variations of the battery SOC are presented in Figure 6(b), while the fuel consumption comparisons between the hybrid railcar (C1) and the pure fuel railcar (C2) are presented in Figure 6(c). With the C-WTVC full-load operation, the demand power (P1), engine output power (P2), and battery output power (P3) for the hybrid railcar can be kept in the range of (-650, 400) kW. Specifically, the battery output power (P3) is relatively stable with the lowest variability among them. The battery SOC varies between 0.595 and 0.630 within a period of 1800 seconds. It should be noted that when compared with the pure gasoline vehicle (C2), which consumes 8070.98 g of fuel, the hybrid railcar in this paper consumes 7493.21 g of fuel, with an improvement of 7.16%.

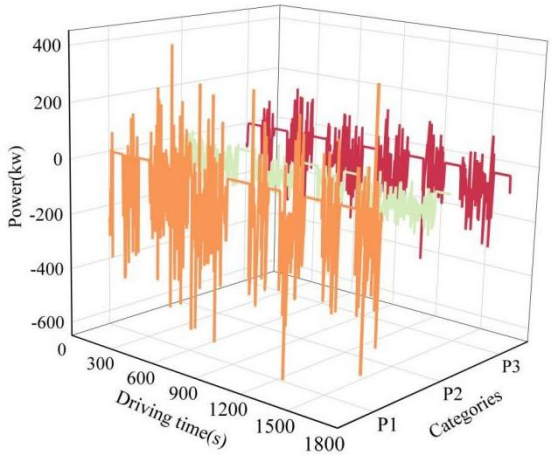

(a) Power distribution curve

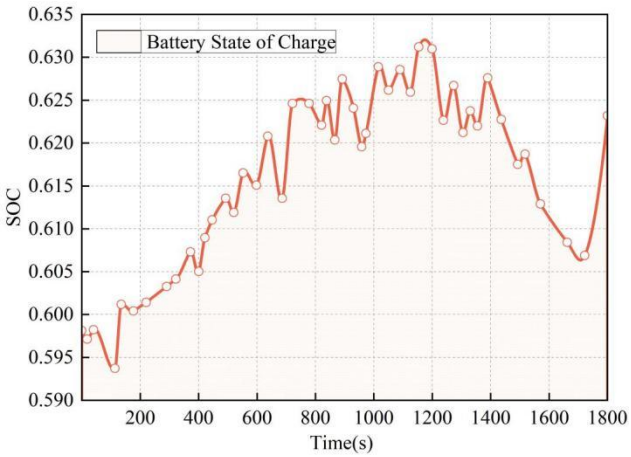

(b) Battery SOC variation

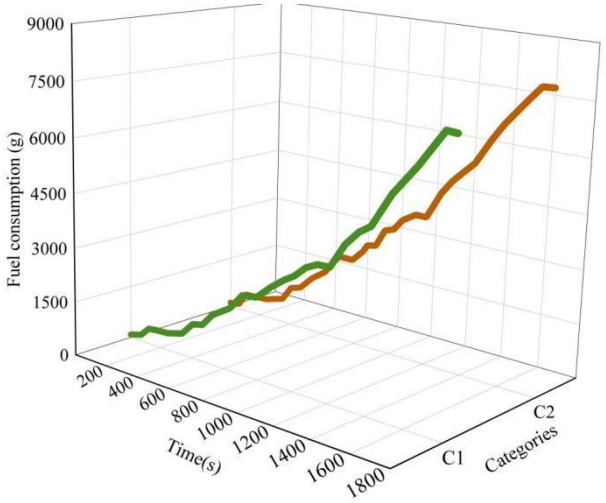

(c) Fuel consumption comparison

Figure 6: Economic performance verification results

4.2 Limitations on Engine Torque Fluctuations

As demonstrated in the previous section, the power performance and fuel efficiency of parallel hybrid vehicles have been further enhanced through the application of multi-objective optimization models. This stems from the energy management strategy's ability to allocate the optimal torque for the vehicle at every instant, achieving instantaneous optimization in energy management at each moment. However, due to the relatively slow response of the engine system in real-world hybrid vehicles, the optimal torque allocation strategy from the previous instant affects the subsequent instant's strategy, leading to frequent large instantaneous torque fluctuations in the engine.

To address the issues of increased fuel consumption, emissions, and reduced engine efficiency caused by large output torque variations, this paper incorporates an engine torque fluctuation constraint model into the energy management control strategy. Assuming no instantaneous change in rotational speed, the model converts engine power variations into equivalent fuel consumption. In the simulation scenario, the WLTC cycle test condition was selected to evaluate engine torque variations during the Coasting Stage (CS). Figure 7 shows engine torque variations before incorporating torque fluctuation limitation. Figure 8 illustrates

engine torque variations after implementing torque fluctuation limitation.

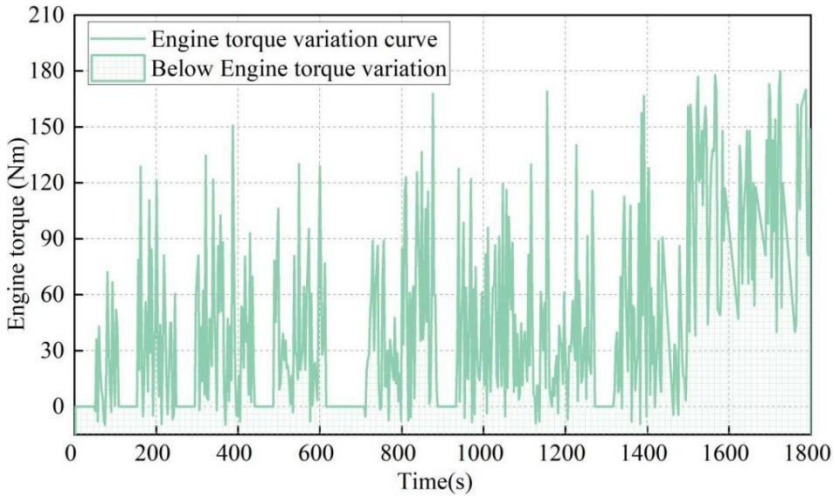

Figure 7: Variations without torque fluctuation limits

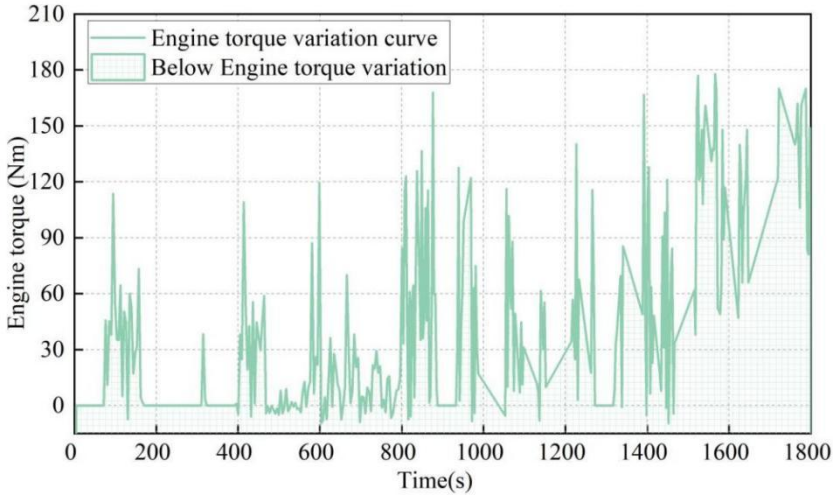

Figure 8: The changes after adding the torque fluctuation limit

By analyzing Figures 7 and 8, one can see that, on average, the relationship between engine torque trends and fuel consumption under conditions of equal fuel consumption with and without torque fluctuation is basically the same. Nevertheless, after introducing the limitation of torque fluctuation, the occurrence of great engine torque fluctuation becomes much rarer, especially during the 0–800 s period when the engine torque fluctuation never exceeds 120 Nm. This occurs because the performance metric requires minimizing the overall fuel consumption at every instant. The mathematical significance of the engine torque fluctuation constraint lies in increasing the equivalent fuel consumption associated with large torque fluctuations. Consequently, determining the torque distribution reduces the likelihood of large torque fluctuations, thereby enhancing engine performance.

4.3 Simulation Experiments and Analysis of Multi-Objective Optimization Models

For solving the optimization problem of energy management for parallel hybrid vehicles based on multi-objective optimization model and algorithm, this paper performs repeated

simulations to obtain multiple optimal solutions. On this basis, 10 typical optimal solution sets are selected and shown in Table 1. Set 1 represents the values of parameters and performance indices before optimization. The selected optimization parameters are P_e: maximum engine power (kW), Nb: number of battery pack modules (blocks), F_d: main transmission ratio, H_{SOC}: upper limit of battery charge (%), L_{SOC}: lower limit of battery charge (%), T_{ch}: battery charging torque (N*m), $K_{\min}$: minimum engine torque coefficient, T_{off}: engine shutdown coefficient, EX_t: initial temperature of catalytic converter (°C), N_n: lower limit of the engine rotational speed (r*min^{-1}), R_o: motor overload coefficient. There are also evaluation indicators Q_{HC}: HC pollutant emissions (g/km), Q_{NO_X}: NOX pollutant emissions (g/km), Q_{CO}: CO pollutant emissions (g/km), $f1$: overall vehicle fuel economy (g/km), $f2$: combined emissions (L/km), $f3$: combined driving performance (m/s3).

Table 1: The optimal result and the values of the optimized parameters

Group	1	2	3	4	5	6	7	8	9	10	11
P_e	41.99	69.69	69.94	68.02	65.33	66.09	70.93	70.98	66.53	46.15	42.41
Nb	2.36	18.50	18.50	17.50	17.50	17.50	20.50	19.50	17.50	17.50	15.50
F_d	1.54	2.14	2.27	2.42	2.29	2.13	2.16	2.15	2.43	2.89	3.48
H_{SOC}	1.23	1.66	1.64	1.64	1.65	1.65	1.66	1.64	1.64	1.77	1.62
L_{SOC}	1.55	1.38	1.35	1.34	1.38	1.41	1.35	1.39	1.34	1.19	1.08
T_{ch}	16.23	22.71	23.42	23.67	23.27	23.09	22.46	22.44	23.67	21.22	24.02
$K_{\min}$	1.38	1.85	1.93	1.94	1.88	1.86	1.83	1.83	1.94	1.57	1.79
T_{off}	0.97	1.16	1.18	1.19	1.19	1.18	1.15	1.14	1.19	1.22	1.20
EX_t	20.98	15.22	15.99	16.36	15.33	15.21	15.19	15.18	16.51	15.29	20.96
N_n	100.46	82.00	82.00	82.00	82.00	82.00	82.00	82.27	81.00	92.00	80.98
R_o	2.78	3.51	3.54	3.53	3.57	3.63	3.4	3.44	3.51	2.5	2.85
Q_{HC}	1.38	1.35	1.35	1.35	1.35	1.35	1.35	1.35	1.35	1.36	1.45
Q_{NO_X}	1.34	1.31	1.3	1.31	1.3	1.31	1.31	1.31	1.31	1.36	1.38
Q_{CO}	3.59	3.07	3.6	3.21	3.69	3.11	3.05	3.02	3.2	3.96	8.63
$f1$	8.49	7.03	6.82	6.93	6.91	6.94	7.12	7.08	6.92	7.32	13.49
$f2$	11.20	10.13	10.45	10.27	10.64	10.17	10.13	10.04	10.26	11.6	17.34
$f3$	217.14	166.51	160.32	196.46	158.52	165.25	166.51	167.46	195.65	148.85	129.99

As can be seen from Table 1, the 10 optimal solution sets selected in this paper have been optimized to a certain extent. Among them, the most concerned $f1$ vehicle fuel economy (g/km) index is improved by 18.60%, and the average value of the selected 10 sets of data is improved by 9.82%. The average optimization degree of $f2$ comprehensive emission (L/km) index is 0.87%, and the average optimization improvement of $f3$ comprehensive driving performance (m/s3) index is 23.76%, which is the largest.

The solution set is chosen randomly for the analysis with the following parameters: variation of SOC, power generation from the engine, power generation of motor, power demand, efficiency points of the engine before and after optimization, and efficiency points of

the motor before and after optimization. Figure 9(a) depicts the comparison of the demanded speed and actual speed. Error obtained by comparing demanded speed and actual speed is illustrated in Figure 9(b). Demand speed and actual speed curves match almost identically and error lies within the range (-0.2, 0.2) s. Therefore, the deviation between the obtained simulation speed and the required speed is minimal and can be considered almost negligible.

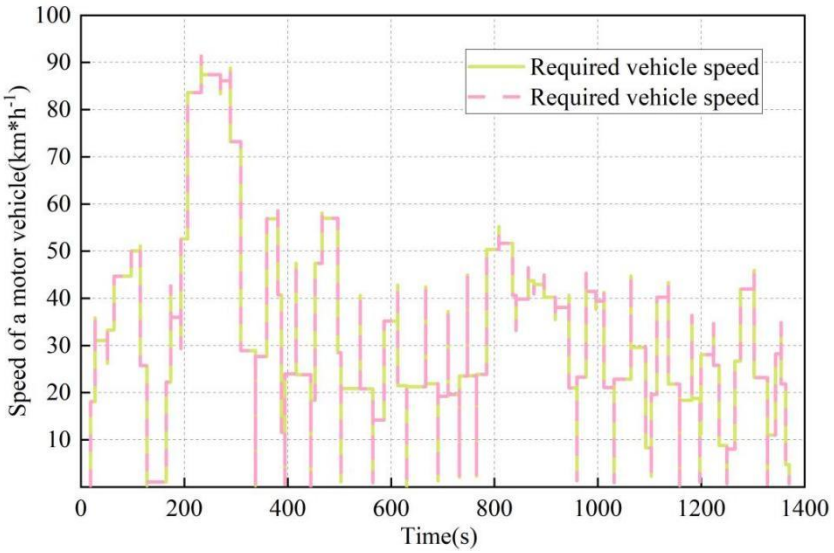

(a) The required speed and the actual speed

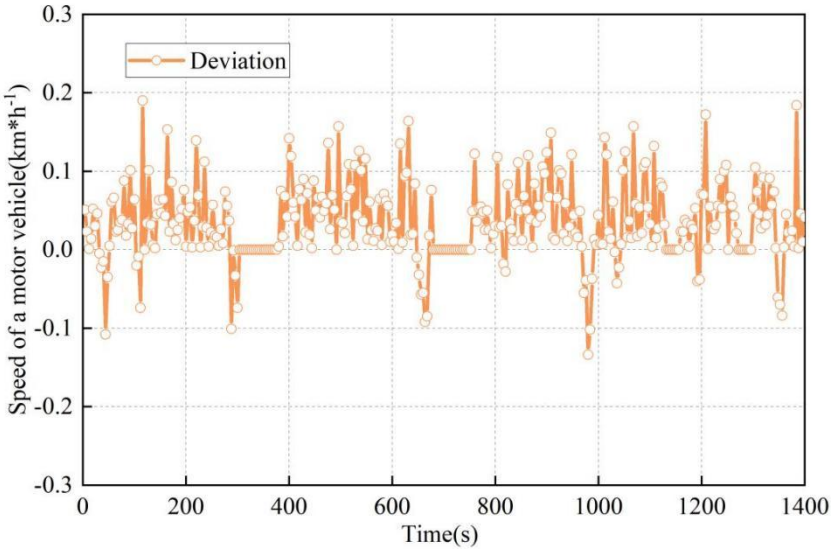

(b) Deviation

Figure 9: Working condition following situation

Further analysis of the power requirements versus motor and engine power reveals the engine efficiency distribution before optimization (A1) and after optimization (A2) as shown in Figure 10. After optimization (A2), the overall operational efficiency of the engine has improved, stabilizing within the 0.20–0.35 range. Low-efficiency points have significantly decreased, and the number of operating points has reduced compared to the pre-optimization state (A1). This reduction is attributed to the multi-objective optimization model employed in this study, which has effectively increased the number of operating points for the motor.

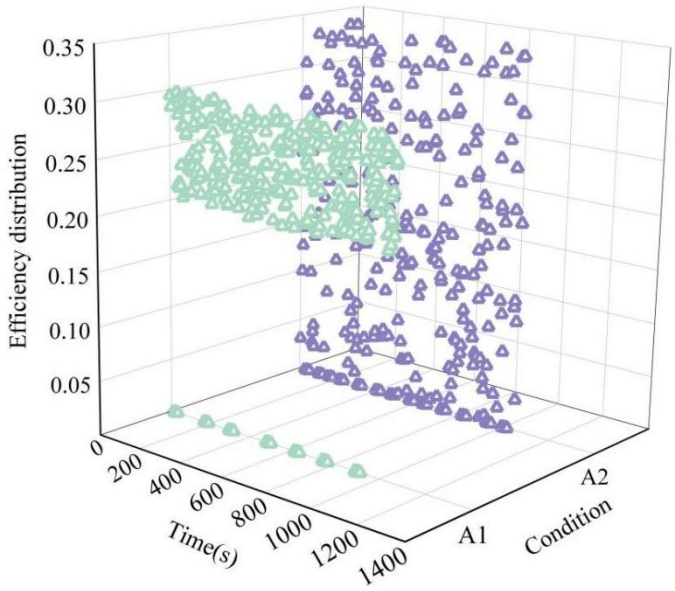

Figure 10: Engine operating point efficiency distribution

As presented in Figure 11, the efficiency distribution of the automotive electric motor working points for before optimization (A1) and after optimization (A2) is depicted. Before optimization (A1), the motor had very good efficiency in the beginning up to 0-400 seconds; however, the efficiency was close to zero thereafter. However, after optimization (A2), there were improvements in the efficiency distributions of the working points of the engine. The primary reason for the shift in the engine's operating point lies in the pre-optimization control strategy, which focused solely on fuel economy to reduce emissions by lowering fuel consumption. However, in actual operation, the fuel-efficient operating region and the emissions-efficient operating region of the engine do not align, preventing emissions optimization. Therefore, the multi-objective optimization method can further enhance engine performance.

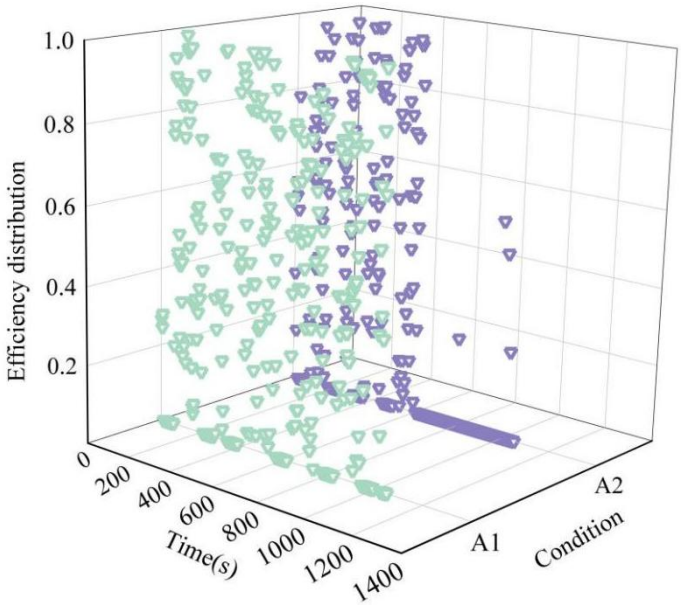

Figure 11: The efficiency distribution at the operating point of the motor

5 Conclusion

This paper constructs an optimization objective function $\min[f(fuel); f(CO); f(HC); f(NOx)]$ based on the operational characteristics of parallel hybrid systems. The initial equivalent factor s_0 is designated as the design variable, with the power battery SOC constraint range set at -3% to 3%. The multi-objective optimization model for energy management strategy of hybrid vehicles based on multi-objective particle swarm optimization algorithm is built up as the selected algorithmic method. Concurrently, an engine torque fluctuation constraint model is introduced to address frequent transient torque fluctuations caused by energy management strategy optimization.

Application experiments of the multi-objective optimization model were conducted on the constructed parallel hybrid vehicle simulation model. For the fully loaded condition, the speed limit of the vehicle model reached 119.37 km/h, higher than the stipulated speed limit of 90 km/h, while the gradient limit reached 42.73% at 10 km/h, surpassing the gradient limit of 20.00% of the base vehicle model. The fuel economy of the vehicle model was enhanced by 7.16% when compared with the pure gasoline vehicle, indicating a good balance between its power performance and economical efficiency. In the research, the multi-objective optimization model established for hybrid vehicles' energy management strategy can provide several optimal solutions for such models, with their fuel economy, overall emissions, and driving performance improved by 9.82%, 0.87%, and 23.76% respectively on average.

About the Author

Quan Huang, a senior engineer, was born in Yulin, Guangxi in 1969. I obtained a bachelor's degree in automotive engineering from Xi'an Institute of Highway (now Chang'an University). I am currently a full-time teacher in the School of Intelligent Manufacturing Engineering of Guangxi Electric Power Vocational and Technical College. My main research direction is mechatronics technology and automotive maintenance technology.

References

[1] Ribeiro, C. B., Rodella, F. H. C., & Hoinaski, L. (2022). Regulating light-duty vehicle emissions: an overview of US, EU, China and Brazil programs and its effect on air quality. Clean Technologies and Environmental Policy, 24(3), 851-862.

[2] Sun, C., Xu, S., Yang, M., & Gong, X. (2022). Urban traffic regulation and air pollution: A case study of urban motor vehicle restriction policy. Energy Policy, 163, 112819.

[3] Filonchyk, M., & Peterson, M. P. (2024). Analysis of air pollution from vehicle emissions for the contiguous United States. Journal of Geovisualization and Spatial Analysis, 8(1), 16.

[4] Meyer, M., Khan, T., Dallmann, T., & Yang, Z. (2023). Particulate matter emissions from US gasoline light-duty vehicles and trucks. United States of America: Washington, DC, USA.

[5] Shen, X., Shi, Y., Kong, L., Cao, X., Li, X., Wu, B., ... & Yao, Z. (2021). Particle number emissions from light-duty gasoline vehicles in Beijing, China. Science of the

Total Environment, 773, 145663.

[6] Lyu, M., Bao, X., Zhu, R., & Matthews, R. (2020). State-of-the-art outlook for light-duty vehicle emission control standards and technologies in China. Clean Technologies and Environmental Policy, 22(4), 757-771.

[7] Zhu, X. H., He, H. D., Lu, K. F., Peng, Z. R., & Gao, H. O. (2022). Characterizing carbon emissions from China V and China VI gasoline vehicles based on portable emission measurement systems. Journal of Cleaner Production, 378, 134458.

[8] Michaux, S. P., Vadén, T., Korhonen, J. M., & Eronen, J. T. (2022). Assessment of the scope of tasks to completely phase out fossil fuels in Finland. Geological Survey of Finland, Report.

[9] Danieli, P., Masi, M., Lazzaretto, A., Carraro, G., Dal Cin, E., & Volpato, G. (2023). Is banning fossil-fueled internal combustion engines the first step in a realistic transition to a 100% RES share?. Energies, 16(15), 5690.

[10] Bresser, D., Hosoi, K., Howell, D., Li, H., Zeisel, H., Amine, K., & Passerini, S. (2018). Perspectives of automotive battery R&D in China, Germany, Japan, and the USA. Journal of Power Sources, 382, 176-178.

[11] Muthukumar, M., Rengarajan, N., Velliyangiri, B., Omprakas, M. A., Rohit, C. B., & Raja, U. K. (2021). The development of fuel cell electric vehicles–A review. Materials Today: Proceedings, 45, 1181-1187.

[12] Lombardi, L., Tribioli, L., Cozzolino, R., & Bella, G. (2017). Comparative environmental assessment of conventional, electric, hybrid, and fuel cell powertrains based on LCA. The International Journal of Life Cycle Assessment, 22(12), 1989-2006.

[13] Conway, G., Joshi, A., Leach, F., García, A., & Senecal, P. K. (2021). A review of current and future powertrain technologies and trends in 2020. Transportation Engineering, 5, 100080.

[14] Hu, D., Wang, Y., Li, J., Yang, Q., & Wang, J. (2021). Investigation of optimal operating temperature for the PEMFC and its tracking control for energy saving in vehicle applications. Energy Conversion and Management, 249, 114842.

[15] Gómez, J. A., & Santos, D. M. (2023). The status of on-board hydrogen storage in fuel cell electric vehicles. Designs, 7(4), 97.

[16] Samsun, R. C., Rex, M., Antoni, L., & Stolten, D. (2022). Deployment of fuel cell vehicles and hydrogen refueling station infrastructure: A global overview and perspectives. Energies, 15(14), 4975.

[17] Chen, Q., Zhang, G., Zhang, X., Sun, C., Jiao, K., & Wang, Y. (2021). Thermal management of polymer electrolyte membrane fuel cells: A review of cooling methods, material properties, and durability. Applied Energy, 286, 116496.

[18] Deng, J., Bae, C., Denlinger, A., & Miller, T. (2020). Electric vehicles batteries: requirements and challenges. Joule, 4(3), 511-515.

[19] Habib, A. A., Hasan, M. K., Issa, G. F., Singh, D., Islam, S., & Ghazal, T. M. (2023). Lithium-ion battery management system for electric vehicles: constraints, challenges, and recommendations. Batteries, 9(3), 152.

[20] Fichtner, M. (2022). Recent research and progress in batteries for electric vehicles. Batteries & Supercaps, 5(2), e202100224.

[21] Huang, Y., Surawski, N. C., Organ, B., Zhou, J. L., Tang, O. H., & Chan, E. F. (2019). Fuel consumption and emissions performance under real driving: Comparison between hybrid and conventional vehicles. Science of the Total Environment, 659, 275-282.

[22] Zhao, J., Xi, X. I., Na, Q. I., Wang, S., Kadry, S. N., & Kumar, P. M. (2021). The technological innovation of hybrid and plug-in electric vehicles for environment carbon pollution control. Environmental Impact Assessment Review, 86, 106506.

[23] Fathabadi, H. (2018). Novel fuel cell/battery/supercapacitor hybrid power source for fuel cell hybrid electric vehicles. Energy, 143, 467-477.

[24] Mustafi, N. N. (2021). An overview of hybrid electric vehicle technology. Engines and Fuels for Future Transport, 73-102.

[25] Krithika, V., & Subramani, C. (2018). A comprehensive review on choice of hybrid vehicles and power converters, control strategies for hybrid electric vehicles. International journal of energy research, 42(5), 1789-1812.

[26] Xue, Q., Zhang, X., Teng, T., Zhang, J., Feng, Z., & Lv, Q. (2020). A comprehensive review on classification, energy management strategy, and control algorithm for hybrid electric vehicles. Energies, 13(20), 5355.

[27] Zhang, F., Wang, L., Coskun, S., Pang, H., Cui, Y., & Xi, J. (2020). Energy management strategies for hybrid electric vehicles: Review, classification, comparison, and outlook. Energies, 13(13), 3352.

[28] Sarvaiya, S., Ganesh, S., & Xu, B. (2021). Comparative analysis of hybrid vehicle energy management strategies with optimization of fuel economy and battery life. Energy, 228, 120604.

[29] Liu, Y., Liu, J., Zhang, Y., Wu, Y., Chen, Z., & Ye, M. (2020). Rule learning based energy management strategy of fuel cell hybrid vehicles considering multi-objective optimization. Energy, 207, 118212.

[30] Du, A., Chen, Y., Zhang, D., & Han, Y. (2021). Multi-objective energy management strategy based on PSO optimization for power-split hybrid electric vehicles. Energies, 14(9), 2438.

[31] Liu, H., Lei, Y., Fu, Y., & Li, X. (2022). A novel hybrid-point-line energy management strategy based on multi-objective optimization for range-extended electric vehicle. Energy, 247, 123357.

[32] Yuan, H. B., Zou, W. J., Jung, S., & Kim, Y. B. (2022). A real-time rule-based energy management strategy with multi-objective optimization for a fuel cell hybrid electric

vehicle. Ieee Access, 10, 102618-102628.

[33] Nassar, M. Y., Shaltout, M. L., & Hegazi, H. A. (2023). Multi-objective optimum energy management strategies for parallel hybrid electric vehicles: A comparative study. Energy conversion and management, 277, 116683.

[34] Zhao, K., He, K., Liang, Z., & Mai, M. (2023). Global optimization-based energy management strategy for series–parallel hybrid electric vehicles using multi-objective optimization algorithm. Automotive Innovation, 6(3), 492-507.

[35] Cheng, J., Yang, F., Zhang, H., Yang, A., & Xu, Y. (2024). Multi-objective adaptive energy management strategy for fuel cell hybrid electric vehicles considering fuel cell health state. Applied Thermal Engineering, 257, 124270.

[36] Lu, Z., Wang, H., He, G., Chen, Y., Li, Z., Zheng, Z., ... & Wang, H. (2025). Optimization framework for multi-objective energy management strategy in hybrid electric vehicles integrating explainable artificial intelligence. Applied Energy, 399, 126484.

[37] Wang, W., Guo, X., Yang, C., Zhang, Y., Zhao, Y., Huang, D., & Xiang, C. (2022). A multi-objective optimization energy management strategy for power split HEV based on velocity prediction. Energy, 238, 121714.

[38] Zhou, L., Yang, D., Zeng, X., Zhang, X., & Song, D. (2023). Multi-objective real-time energy management for series–parallel hybrid electric vehicles considering battery life. Energy Conversion and Management, 290, 117234.

[39] Sellali, M., Ravey, A., Betka, A., Kouzou, A., Benbouzid, M., Djerdir, A., ... & Abdelrahem, M. (2022). Multi-objective optimization-based health-conscious predictive energy management strategy for fuel cell hybrid electric vehicles. Energies, 15(4), 1318.

[40] Hou, S., Chen, H., Yin, H., Zhao, J., Xu, F., & Gao, J. (2024). Energy Management Based on Mixed-Integer Nonlinear Model Predictive Control for Hybrid Electric Vehicles. IEEE Transactions on Intelligent Transportation Systems.

[41] Li, D., Zhang, J., & Jiang, D. (2024). Energy management of hybrid electric vehicle based on linear time-varying model predictive control. International Journal of Powertrains, 13(1), 95-111.

[42] Zheng, C., Zhang, D., Xiao, Y., & Li, W. (2022). Reinforcement learning-based energy management strategies of fuel cell hybrid vehicles with multi-objective control. Journal of Power Sources, 543, 231841.

[43] Deng, P., Wu, X., Yang, J., Yang, G., Jiang, P., Yang, J., & Bian, X. (2024). Optimal online energy management strategy of a fuel cell hybrid bus via reinforcement learning. Energy Conversion and Management, 300, 117921.

[44] Montaleza, C., Arévalo, P., Gallegos, J., & Jurado, F. (2024). Enhancing energy management strategies for extended-range electric vehicles through deep Q-learning and continuous state representation. Energies, 17(2), 514.

[45] Shi, D., Xu, H., Wang, S., Hu, J., Chen, L., & Yin, C. (2024). Deep reinforcement learning based adaptive energy management for plug-in hybrid electric vehicle with double deep Q-network. Energy, 305, 132402.

[46] Wang, Z., Zhang, S., Luo, W., & Xu, S. (2024). Deep reinforcement learning with deep-Q-network based energy management for fuel cell hybrid electric truck. Energy, 306, 132531.

[47] Zhou, J., Feng, C., Su, Q., Jiang, S., Fan, Z., Ruan, J., ... & Hu, L. (2022). The multi-objective optimization of powertrain design and energy management strategy for fuel cell–battery electric vehicle. Sustainability, 14(10), 6320.

[48] Qin, J., Huang, H., Lu, H., & Li, Z. (2025). Energy management strategy for hybrid electric vehicles based on deep reinforcement learning with consideration of electric drive system thermal characteristics. Energy Conversion and Management, 332, 119697.

[49] Li, X., Zhou, Z., Wei, C., Gao, X., & Zhang, Y. (2025). Multi-objective optimization of hybrid electric vehicles energy management using multi-agent deep reinforcement learning framework. Energy and AI, 20, 100491.